04-82-74

Materials Science and Engineering, 56 (1982) 135 - 141

Influence of the Sample Radius and Irradiated Zone Width on the Defocusing Phenomenon in the Schulz Technique

J. D. HERMIDA

Comision Nacional de Energia Atomica, Departamento de Materiales, 1429 Buenos Aires (Argentina)

(Received February 17, 1982)

SUMMARY

The influence of the sample radius and irradiated zone width on the defocusing phenomenon is analysed by means of theoretical expressions which result from the convolution of a Cauchy fitting of the diffraction peak on the receiving plane. For the usual sample radius (about 12 mm) an irradiated zone width which is larger than expected may be used without any additional intensity loss. For a small sample radius (e.g. 4 mm), defocusing is less pronounced when a 6 mm irradiated zone width is used. (0002) and {10$\bar{1}$0} pole figures of Zry-4 (a zirconium-based alloy) samples illustrate the results.

1. INTRODUCTION

In previous work, Ortiz and Hermida [1] derived a theoretical expression for correcting the diffracted intensities for defocusing in the Schulz technique. The analysis was based on the assumption that the irradiated zone remained within the sample limits during the whole experiment. For a circular sample of radius about 0.5 in, in the diffraction angle range (10° - 20°) usually used for texture determination the initial irradiated zone width should not exceed 6 mm. A reduction in the sample radius would require a beam width reduction, but the diffracted intensity would also decrease appreciably.

Tensile and creep samples, for example, usually are about 3 - 6 mm wide. To obtain a sample suitable for texture determination, several of these small samples collected together to form a layer sample would be needed; this would be very time consuming. Therefore, if small samples and no initial intensity reduction are required simultaneously, a new source of intensity decrease which arises when the sample is tilted has to be taken into account: the fact that the irradiated zone is larger than the sample radius.

2. THEORY

2.1. Sample radius larger than irradiated zone width

In Fig. 1 a side view of the tilted sample is shown. The height of the X-ray beam is h, $h\alpha$ is half the vertical component of its projection on the sample and $x\alpha$ is the maximum separation of the irradiated zone from the vertical plane for $\alpha = 0$. The irradiated zone viewed from the normal direction to the sample is shown in Fig. 2. The irradiated zone width defined by $2a$ and $h\theta$ is the horizontal component of the beam projection. The following expressions are easily established:

$$h\alpha = \frac{h}{2\cos\alpha}$$

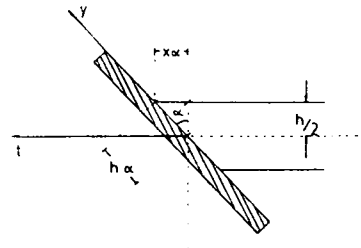

Fig. 1. Side view of a tilted sample used for the Schulz technique.

0025-5416/82/0000-0000/$02.75

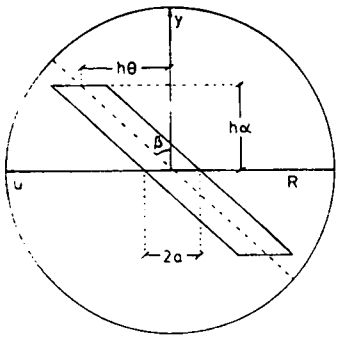

Fig. 2. Irradiated zone viewed from the normal direction to the tilted sample.

$$x\alpha = \frac{h}{2}\tan\alpha$$

$$h\theta = \frac{x\alpha}{\tan\theta}$$

$$\tan\beta = \frac{h\theta}{h\alpha} = \frac{\sin\alpha}{\tan\theta}$$

The irradiated zone will remain within the sample limits until

$$h\alpha\tan\beta + a > (R^2 - h^2\alpha)^{1/2}$$

where R is the sample radius. Until then the total diffracted intensity is the convolution (on the receiving plane) or the diffracted intensity of each differential of the irradiated zone area [1, 2]:

$$I(x) = \frac{1}{2h\alpha(2a)}\int_{-h\alpha}^{h\alpha} i\{x - x'(y)\}(2a)\,dy$$

where $x'(y) = y\tan\beta\sin\theta + y\sin\alpha\cos\theta = 2y\sin\alpha\cos\theta$ and $i(x)$ is the intensity profile (Fig. 3). However, if the irradiated zone does not remain within the surface limits, as is shown in Fig. 4, the centre of each differential of irradiated zone area is shifted towards the vertical axis; y denotes its position which is determined from

$$u = \frac{y\tan\beta + (R^2 - y^2)^{1/2} - a}{2}$$

and its width is given by

$$\overline{AB} = a + (R^2 - y^2)^{1/2} - y\tan\beta$$

Therefore, as can be seen in Fig. 3, the new variable x'' is given by

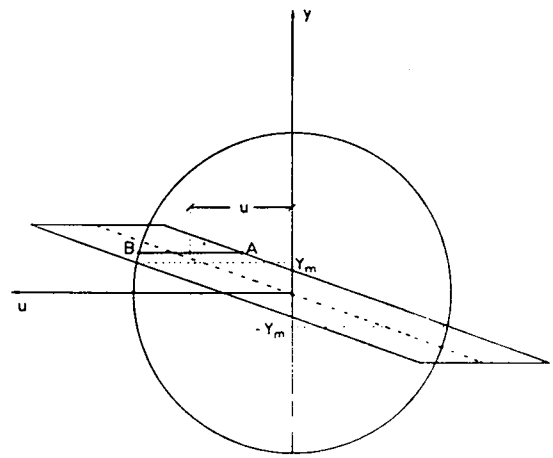

Fig. 3. Schematic top view of the focusing condition when the sample is tilted.

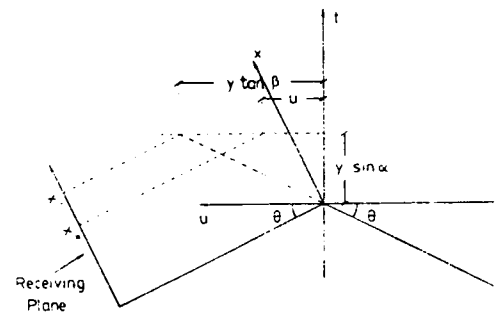

Fig. 4. A schematic diagram showing when the irradiated zone no longer remains within the sample limits.

$$x''(y) = u\sin\theta + y\sin\alpha\cos\theta$$

$$= \frac{3y\sin\alpha\cos\theta + \{(R^2 - y^2)^{1/2} - a\}\sin\theta}{2}$$

The lower integration limit y_m corresponding to this case is obtained from the expression (Fig. 4)

$$y_m\tan\beta + a = (R^2 - y_m^2)^{1/2}$$

which gives

$$y_m = \frac{\{(R^2 - a^2) + R^2\tan^2\beta\}^{1/2} - a\tan\beta}{\tan^2\beta + 1}$$

When the condition

$$h\alpha\tan\beta - a < (R^2 - h^2\alpha)^{1/2}$$

is fulfilled, the upper integration limit is

$$Y_M = h\alpha$$

In other cases, Y_M must be obtained from

$$Y_M\tan\beta - a = (R^2 - y_M^2)^{1/2}$$

which gives

$$Y_M = \frac{\{(R^2 - a^2) + R^2 \tan^2\beta\}^{1/2} + a \tan\beta}{\tan^2\beta + 1}$$

Then the total diffracted intensity is given by

$$I(x) = I_1(x) + I_2(x) + I_3(x)$$

where

$$I_1(x) = \frac{1}{4h\alpha a} \int_{Y_m}^{Y_M} i\left[x + \frac{\{(R^2 - y^2)^{1/2} - a\}\sin\theta + 3y \sin\alpha\cos\theta}{2}\right]\{a + (R^2 - y^2)^{1/2} - y\tan\beta\}\,dy$$

$$I_2(x) = \frac{1}{2h\alpha} \int_{-y_m}^{y_m} i(x - 2y\sin\alpha\cos\theta)\,dy$$

and

$$I_3(x) = \frac{1}{4h\alpha a} \int_{y_m}^{y_M} i\left[x - \frac{\{(R^2 - y^2)^{1/2} - a\}\sin\theta + 3y \sin\alpha\cos\theta}{2}\right]\{a + (R^2 - y^2)^{1/2} - y\tan\beta\}\,dy$$

The defocusing factor is expressed by

$$F(\alpha) = \int_{-W_R/2}^{W_R/2} I(x)\,dx \Big/ \int_{-W_R/2}^{W_R/2} i(x)\,dx$$

where W_R is the receiving slit width.

2.2. Sample radius smaller than irradiated zone width

This new case is represented in Fig. 5. When

$$h\alpha\tan\beta < a - (R^2 - h\alpha)^{1/2}$$

(*i.e.* zone 1), the diffracted intensity is given by

$$I(x) = \frac{1}{2h\alpha a} \int_{-h\alpha}^{h\alpha} i(x - y\sin\alpha\cos\theta)(R^2 - y^2)^{1/2}\,dy$$

When this condition is no longer fulfilled (*i.e.* zone 2),

$$I(x) = I_1(x) + I_2(x) + I_3(x)$$

with

$$I_1(x) = \frac{1}{4h\alpha a} \int_{y_0}^{h\alpha} i\left[x - \frac{\{(R^2 - y^2)^{1/2} - a\}\sin\theta + 3y \sin\alpha\cos\theta}{2}\right]\{a + (R^2 - y^2)^{1/2} - y\tan\beta\}\,dy$$

$$I_2(x) = \frac{1}{2h\alpha a} \int_{-y_0}^{y_0} i(x - y\sin\alpha\cos\theta)(R^2 - y^2)^{1/2}\,dy$$

$$I_3(x) = \frac{1}{4h\alpha a} \int_{y_0}^{h\alpha} i\left[x + \frac{\{(R^2 - y^2)^{1/2} - a\}\sin\theta + 3\sin\alpha\cos\theta}{2}\right]\{a + (R^2 - y^2)^{1/2} - y\tan\beta\}\,dy$$

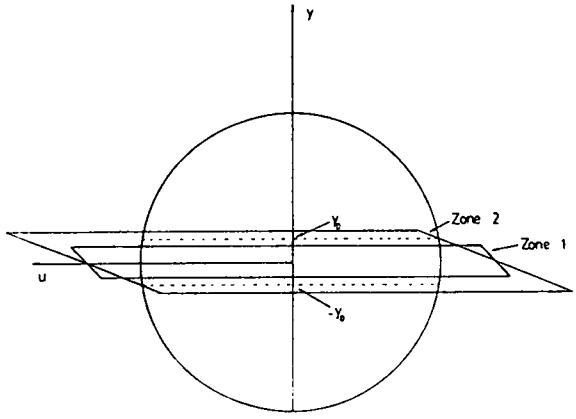

Fig. 5. Irradiated zone viewed from the normal direction to the tilted sample for $a > R$.

where y_0 is found through the expression (Fig. 5)

$$a - y_0 \tan\beta = (R^2 - y_0^2)^{1/2}$$

which gives

$$y_0 = \frac{a\tan\beta - \{R^2\tan^2\beta - (a^2 - R^2)\}^{1/2}}{\tan^2\beta + 1}$$

In this case the diffracted intensity for $\alpha = 0$ is given by

$$I_0(x) = \frac{1}{ha}\int_{-h/2}^{h/2} i(x)(R^2 - y^2)^{1/2}\,dy$$

$$= \frac{1}{ha}\left[\frac{h}{2}\left\{R^2 - \left(\frac{h}{2}\right)^2\right\}^{1/2} + R^2\sin^{-1}\left(\frac{h}{2R}\right)\right] i(x)$$

3. CALCULATION

In both cases the integrals $I_1(x)$ and $I_3(x)$, and also the integral $I_2(x)$ in the case described in Section 2.2, had to be solved numerically and Simpson's rule was employed. The intensity profiles $i(x)$ were given by Cauchy fittings [1] and the misalignment factors [3] were also included. For this purpose, a FORTRAN IV program was developed for use with an IBM 370 computer. The $F(\alpha)$ factors were finally calculated as a function of the tilt angle in 2.5° steps. The program uses 234k storage locations and consists of 249 instructions.

Copies of this program and any additional information may be obtained from the author.

To show the variation in the curves of the defocusing coefficient $F(\alpha)$ with the sample radius R and the irradiated zone width $2a$, two extreme values of R were chosen, 4 and 12 mm. The values of θ and K (a constant of the Cauchy fitting) were chosen as those corresponding to the (0002) peak, for copper radiation, of zirconium samples. In Fig. 6,

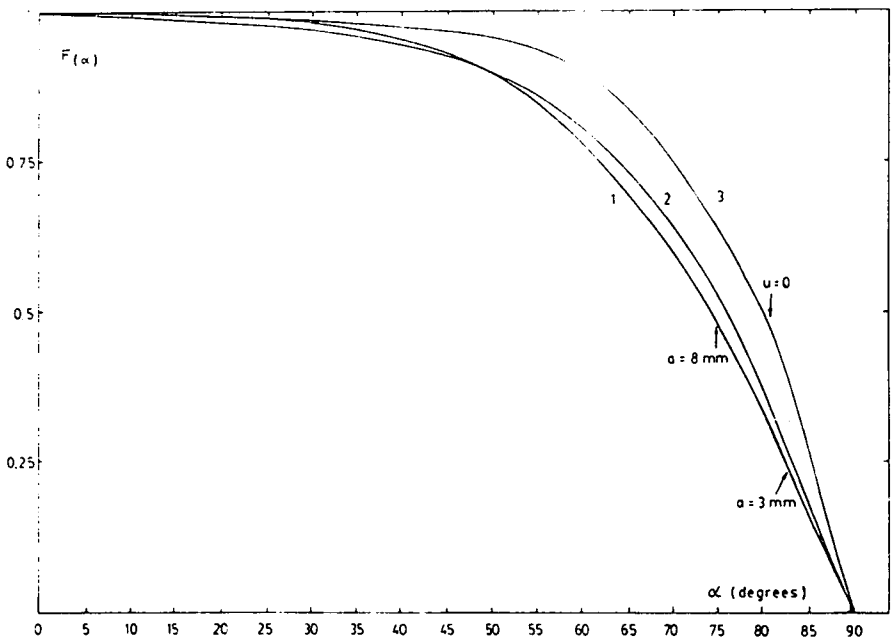

Fig. 6. Defocusing coefficient $F(\alpha)$ as a function of the tilt angle α, for a sample radius R of 12 mm: curve 1, a = 3 mm, a = 8 mm; curve 2, a = 12 mm; curve 3, a = 18 mm.

three curves corresponding to four different values of a for R = 12 mm are shown. Curve 1 corresponds to a = 3 mm and a = 8 mm, curve 2 to a = 12 mm and curve 3 to a = 18 mm. In Fig. 7, three curves corresponding to a = 2 mm, a = 4 mm and a = 6 mm for R = 4 mm are shown. In both figures the arrows indicate the values of the tilt angle α_{LIM} at which the irradiated zone no longer remains within the limits of the sample surface. For R = 4 mm the shapes of the curves as functions of a are quite different. The curve for a = 2 mm coincides up to α = 63° with the curve (the "original" curve) for which the sample radius and the irradiated zone width are not taken into account (dotted line). At angles slightly larger than this, the irradiated zone no longer remains totally within the sample surface, and there is an additional intensity decrease; this becomes marked from α = 75°. This angle also corresponds to a value of α_{LIM} for a small irradiated zone halfwidth such as a = 0.1 mm, indicating that it is impossible to avoid this new source of intensity loss for R = 4 mm. For a = 4 mm there is a marked intensity decrease starting from $\alpha \mp 0$ because, for small angles, defocusing is not significant and the fact that the irradiated zone no longer remains within the sample limits becomes the only reason for the occurrence of this decrease. The difference between curves 1 and 2 increases up to about α = 35° and then, as defocusing becomes increasingly pronounced, it decreases progressively. In contrast, for a = 6 mm (curve 3), up to α = 64°,

$$h\alpha \tan\beta < a - (R^2 - h\alpha^2)^{1/2}$$

i.e. the centre of each differential of the irradiated zone area is situated on the y axis (u = 0 in Fig. 5); defocusing is even smaller than for a = 2 mm (curve 1). For this and larger angles the difference between the two curves becomes smaller as defocusing begins to play the dominant role. For R = 12 mm the curves for a = 3 mm and a = 8 mm coincide with the original curve. It is interesting to note that, even for a = 8 mm with α_{LIM} = 75°, the effect caused by the fact that the zone is not within the sample limits is negligible compared with defocusing and consequently there is no additional intensity loss. For a = 12 mm there is an additional intensity loss, from α = 0, for R = a = 4 mm but, from α = 50°, the situation is reversed because defocusing is smaller than for a = 8 mm. For R = 18 mm the curve behaves similarly to the curve for R = 4 mm and a = 6 mm.

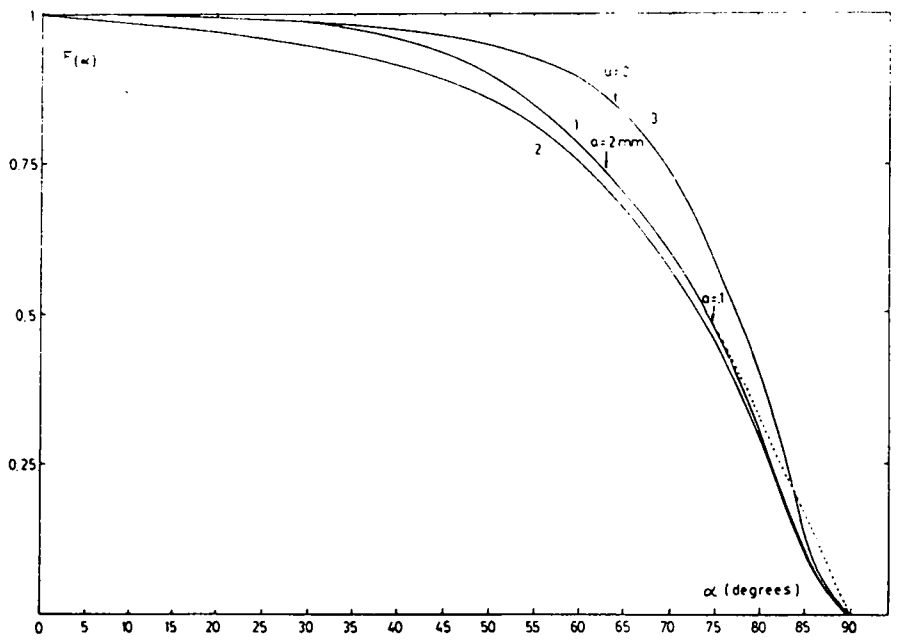

Fig. 7. Defocusing coefficient $F(\alpha)$ as a function of the tilt angle α, for a sample radius R of 4 mm: curve 1, a = 2 mm; curve 2, a = 4 mm; curve 3, a = 6 mm.

4. EXPERIMENTAL DETAILS

Two sets of complete pole figures ((0002) and $\{10\bar{1}0\}$) for Zry-4 (a zirconium-base alloy used for cladding the tubes of fuel elements in pressurized water reactors) were obtained.

A standard Siemens texture goniometer with filtered copper radiation was employed. Misalignment conditions were analysed and Δd and Δh values similar to those obtained in the work of Ortiz and Hermida [1] were obtained. A 5° spiral was chosen and consequently, to cover the whole projection, the receiving slit height was fixed according to the following equation [4]:

$$\Delta\alpha = \frac{W_H}{2r \sin\theta}$$

where W_H is the receiving slit height, r is the goniometer radius and $\Delta\alpha$ is the tilt angle

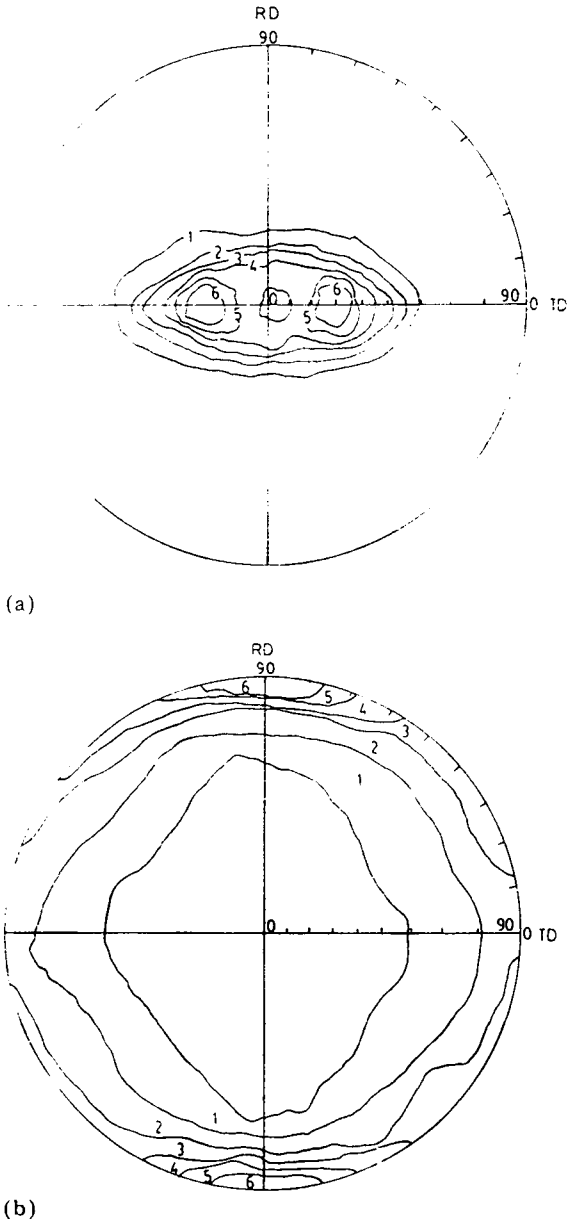

Fig. 8. (a) (0002) and (b) $\{10\bar{1}0\}$ pole figures for a Zry-4 cladding tube sample (RD, rolling direction; TD, tensile direction).

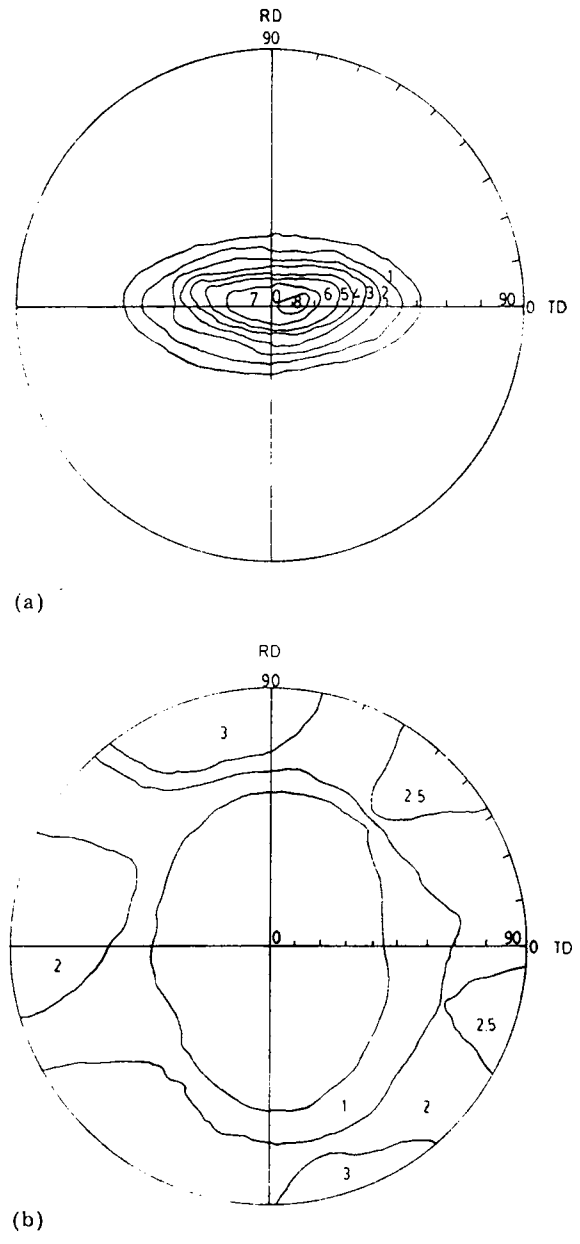

Fig. 9. (a) (0002) and (b) $\{10\bar{1}0\}$ pole figures for an annealed Zry-4 sheet sample which had been cold rolled and stress relieved (RD, rolling direction; TD, tensile direction).

interval for the incident diffracted intensity. The intensities were collected in 5 s intervals until $\alpha = 87.5°$ was reached; these intensities were corrected for defocusing using the corresponding theoretical expressions.

In Fig. 8 the (0002) and $\{10\bar{1}0\}$ pole figures of a Zry-4 sample obtained from a cladding tube are shown. This sample had a radius of 12 mm and according to previous results an irradiated zone width of 8 mm was chosen to increase the intensity and to improve the counting statistics.

In Fig. 9, another set of (0002) and $\{10\bar{1}0\}$ pole figures is shown. In this case the sample was obtained from an annealed creep sample (1 h at 800 °C) 4 mm wide and 40 mm long that had been drawn from a cold-rolled (64%) and stress-relieved (2 h at 520 °C) Zry-4 sheet. Two pieces 4 mm long of the creep sample were put together to make a circular texture sample 8 mm long.

The pole figures in Fig. 8 have the characteristics expected from this type of samples [5] and it should be pointed out that there is good definition between pole density levels close to $\alpha = 90°$.

In the (0002) pole figure in Fig. 9 the maximum pole density is concentrated near the normal direction, as is expected because of the annealing process; in the $\{10\bar{1}0\}$ pole figure in Fig. 9 the six prism poles are more clearly defined and the $\langle 11\bar{2}0\rangle$ direction tends to be aligned with the rolling direction [5].

5. CONCLUSIONS

Although calculations and experiments have been performed for only one diffraction angle, $\theta = 17.4°$, the analysis is quite general and several conclusions can be drawn. With the usual sample diameter, about 24 mm, the diffracted intensity can be increased, and consequently also the pole figure accuracy, by means of a larger irradiated zone width without any additional intensity loss.

Smaller samples can be analysed with good results, and for any case an irradiated zone width larger than the sample radius is advisable.

This work and the earlier work of Ortiz and Hermida [1] show the reliability of the Schulz technique for obtaining complete pole figures, provided that all the misalignment and defocusing factors are carefully analysed and taken into account.

REFERENCES

1 M. Ortiz and J. D. Hermida, *Texture*, *4* (1981) 159.
2 A. Segmuller, *J. Appl. Phys.*, *43* (1972) 2907.
3 M. Ortiz and J. D. Hermida, *Texture*, *4* (1980) 57.
4 J. Couterne and G. Cizeron, *J. Appl. Crystallogr.*, *4* (1971) 461.
5 E. Tenckhoff and P. Rittenhouse, *J. Nucl. Mater.*, *35* (1970) 14.